THE JOURNAL OF PHYSICAL CHEMISTRY B

Article

pubs.acs.org/JPCB

Molecular Simulations of Hydrogen Bond Cluster Size and Reorientation Dynamics in Liquid and Glassy Azole Systems

Qinfang Sun,[†] Jacob A. Harvey,[§] Katharine V. Greco,[†] and Scott M. Auerbach*[,†,‡]

[†]Department of Chemistry, University of Massachusetts, Amherst, Massachusetts 01003, United States

[‡]Department of Chemical Engineering, University of Massachusetts, Amherst, Massachusetts 01003, United States

[§]Department of Chemistry, University of Kansas, Lawrence, Kansas 66045, United States

Supporting Information

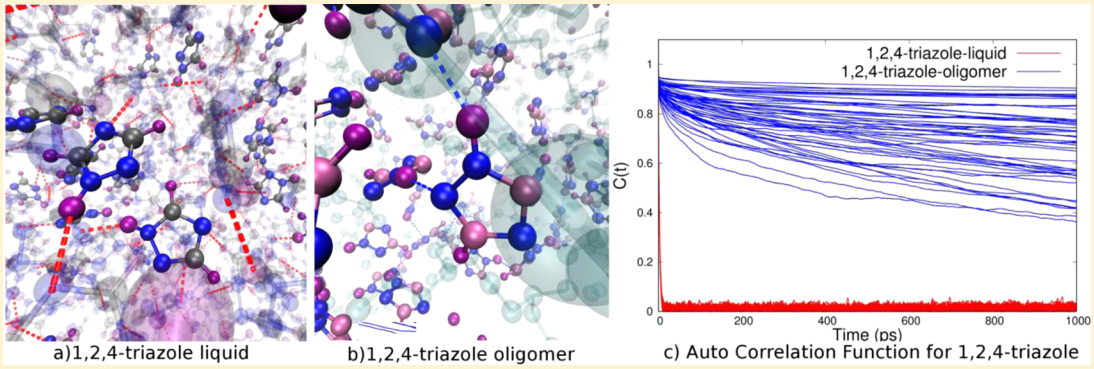

ABSTRACT: We simulated the dynamics of azole groups (pyrazole, imidazole, 1,2,3-triazole, 1,2,4-triazole, and tetrazole) as neat liquids and tethered via linkers to aliphatic backbones to determine how tethering and varying functional groups affect hydrogen bond networks and reorientation dynamics, both factors which are thought to influence proton conduction. We used the DL_Poly_2 molecular dynamics code with the GAFF force field to simulate tethered systems over the temperature range 200−900 K and the corresponding neat liquids under liquid state temperatures at standard pressure. We computed hydrogen bond cluster sizes; orientational order parameters; orientational correlation functions associated with functional groups, linkers, and backbones; time scales; and activation energies associated with orientational randomization. All tethered systems exhibit a liquid to glassy-solid transition upon cooling from 600 to 500 K, as evidenced by orientational order parameters and correlation functions. Tethering the azoles was generally found to produce hydrogen bond cluster sizes similar to those in untethered liquids and hydrogen bond lifetimes longer than those in liquids. The simulated rates of functional group reorientation decreased dramatically upon tethering. The activation energies associated with orientational randomization agree well with NMR data for tethered imidazole systems at lower temperatures and for tethered 1,2,3-triazole systems at both low- and high-temperature ranges. Overall, our simulations corroborate the notion that tethering functional groups dramatically slows the process of reorientation. We found a linear correlation between gas-phase hydrogen bond energies and tethered functional group reorientation barriers for all azoles except for imidazole, which acts as an outlier because of both atomic charges and molecular structure.

1. INTRODUCTION

The past decade has seen significant research on tethered hydrogen bonded systems for understanding a variety of phenomena, including proton conduction in proton exchange membranes (PEMs),[1−5] biological proton shuttling,[6−8] and organic material self-assembly.[9−12] Focusing on proton conduction in PEMs, there has been intense research on materials composed of tethered amphiprotic functional groups where unidirectional proton conduction is thought to follow the Grotthuss mechanism involving two steps:[1,13] facile multigroup proton jumps, followed by more sluggish functional group reorientations to allow subsequent proton conduction. This two-step mechanism complicates the design of advanced materials because of two competing hydrogen bonding effects:[14,15] strong hydrogen bonding producing larger clusters of hydrogen bonded functional groups, allowing longer proton jumps, and weaker hydrogen bonding, allowing more rapid functional group reorientation. Tethering of functional groups generally causes proton conductivities to drop by orders of magnitude from corresponding neat liquid values,[1] warranting a deeper fundamental understanding of the tethering effect on hydrogen bonding in such systems. In this article, we report classical molecular dynamics simulations on various azole systems to study the effects of tethering and of varying

Received: July 18, 2016
Revised: September 13, 2016
Published: September 15, 2016

DOI: 10.1021/acs.jpcb.6b07148
J. Phys. Chem. B 2016, 120, 10411−10419

functional groups to discover trends in hydrogen bonded cluster sizes and functional group reorientation rates in glassy and liquid systems.

Understanding the structures and dynamics of tethered hydrogen bonding systems in the absence of excess charge is an important precursor to a fuller consideration of charge transport through such systems.[14−16] Materials comprised of tethered amphiprotic groups can exist in crystalline,[15,17−19] glassy,[2,20−22] and liquid/molten[23−25] states, raising the question of how phase changes may influence the nature of hydrogen bond networks in tethered systems. From a molecular standpoint, tethering functional groups involves the addition of backbone and/or linker moieties, each with its own relaxation time scales. This suggests fundamental questions about the hierarchies of relaxation time scales for functional group, linker, and backbone species and how they vary among systems.[26−28] This last issue is particularly relevant for designing new proton exchange materials. In particular, polymer chemists often strive to synthesize materials with low glass-transition temperatures to retain segmental flexibility and liquid-like dynamics that often give rise to higher proton conductivities.[4] However, it is not obvious how backbone flexibility, which is related to the glass-transition, correlates with functional group dynamics, which in turn is related to hydrogen bond and proton motion. In the present work, we address these issues by simulating the energetics associated with reorientation of functional group, linker, and backbone species in liquid and tethered azole systems.

A variety of NMR measurements of spin−lattice and spin−spin relaxation times have yielded important information on hydrogen bond dynamics for tethered functional groups. In particular, Spiess and co-workers have applied magic angle spinning (MAS) solid-state NMR methods to study the hydrogen bond dynamics of imidazole[29] and triazole[30] groups tethered in various ways, finding the presence of both high- and low-temperature phases with very different apparent activation energies for functional group rotational motion. For the imidazole-based system, Spiess and co-workers studied materials composed of imidazole pairs linked by ether groups of various lengths and found disordered domains with molecules in a state of fluctuating hydrogen bonding along with ordered domains with more static hydrogen bonding,[29] raising a question about the nature of these different environments. Spiess and co-workers also applied solid-state NMR to study 1,2,3-triazole tethered to a siloxane polymer, finding a low-temperature phase with an apparent activation energy for functional group rotation of 58 kJ/mol and a high-temperature activation energy of 31 kJ/mol,[30] raising a question about why these activation energies are so different. We apply molecular dynamics simulations to address these qualitative and quantitative experimental findings to shed new light on hydrogen bonding in tethered systems.

The synthetic chemistry of tethering amphiprotic functional groups utilizes a great variety of chemical species as flexible linkers and backbones.[30−32] To model such systems with one simple and computationally tractable approach, we studied herein and in previous work[14,15,33] the dynamics of materials composed of oligomers, i.e., short brush-like molecules[34] with flexible alkane backbones and short alkyl linkers that connect functional groups to backbones (see Figure 1). We showed in earlier work that pentamer brushes with such an architecture balance material stability and molecular flexibility.[14,15] Below, we investigate the competition between hydrogen bond network stability and flexibility in liquids and glassy materials composed of pentamer brushes. Regarding functional groups, the nitrogenous heterocycle imidazole has gained attention because imidazole (the side chain in the amino acid histidine) is found in many proton shuttling proteins.[6,35] Other azoles such as pyrazole, triazole, and tetrazole have also been studied to determine how the number and positioning of nitrogen in the heterocycle influence proton motion.[25,36−38] A systematic study considering these functional groups[22,39−43] is important for elucidating how the trade-off between hydrogen bonding networks and functional group reorientation varies among these systems. In addition, a systematic study comparing untethered and tethered materials[16,31,39,44] comprising these functional groups can shed light on how tethering impacts the trade-off between hydrogen bond network formation and reorientation dynamics. We present such a systematic study below using classical molecular dynamics.

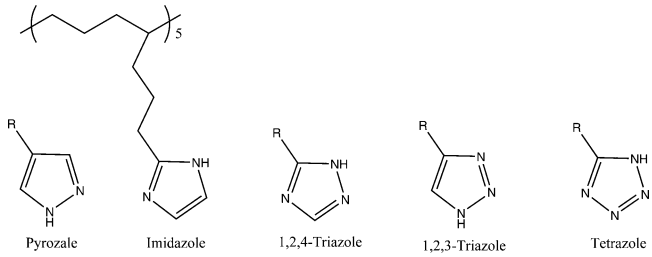

Figure 1. Oligomer with a butyl backbone, propyl linker, and various functional groups.

Below, we find that tethered systems exhibit the same sizes of hydrogen bond clusters as in untethered systems, except with longer hydrogen bond lifetimes upon tethering. Simulated rates of functional group reorientation reported below decreased dramatically upon tethering. The computed activation energies associated with orientational randomization show good agreement with NMR data in the tethered imidazole system at low temperatures and with the 1,2,3-triazole oligomer system in both low- and high-temperature regimes.

The remainder of this article is organized as follows: Section 2 presents the theoretical and simulation methods applied below; Section 3 details the results and discussion on hydrogen bonding in liquid and glassy systems, and Section 4 offers a summary and concluding remarks. We also include Supporting Information with additional simulation data.

2. THEORETICAL METHODS

Systems. We modeled molecular oligomers with the following pendant functional groups: pyrazole, imidazole, 1,2,4-triazole, 1,2,3-triazole, and tetrazole (see Figure 1). Each monomer unit includes an amphiprotic group tethered to a butyl backbone by a propyl linker (Figure 1). Our previous work[14,15,33] and Cavalcanti[45] showed that such backbone/linker groups are the shortest ones that provide enough configurational freedom for strong hydrogen bonding between amphiprotic groups. As such, these backbone/linker chains allow for ample hydrogen bonding while excluding relatively small volume fractions. In addition, such alkyl chains can be described by well-established potential parameters. In previous work,[14,15,33] we considered oligomers with pendant imidazole of lengths ranging from n = 1 to 10, finding that pentamers provide an interesting and potentially useful balance between solid-like mechanical stability and liquid-like molecular

DOI: 10.1021/acs.jpcb.6b07148
J. Phys. Chem. B 2016, 120, 10411−10419

flexibility. In what follows, we focus on five materials composed of pentamers, each with one of the five pendant amphiprotic groups.

We also considered five neat liquids, each composed of the amphiprotic groups shown in Figure 1 with R replaced by hydrogen. The five pentamer-based systems were simulated at temperatures from 200 to 900 K, while the neat liquids were studied at temperatures between the known standard melting and boiling temperatures for each liquid.

Each liquid system was formed by starting with the crystal structure of the corresponding molecular solid, if available in the Cambridge Structural Database (CSD),[46] and performing the sequence of steps listed below. All simulations were carried out using DL_Poly_2, as in our previously reported work on these systems.[14,15] When a crystal structure was not found in the CSD, we constructed a plausible unit cell using interatomic distances extracted from analogous systems. Beginning with each unit cell, we performed the following steps:

(i) Periodic extension in three-dimensions to yield a system with at least 500 molecules and with lattice parameters in all directions of at least 30 Å.
(ii) Truncation into an orthorhombic simulation box with lattice parameters of at least 30 Å, deleting a small number of molecules outside the orthorhombic simulation cell while retaining close to 500 molecules in all cases to yield an initial condition for energy minimization.
(iii) Energy minimization at constant (orthorhombic) volume to yield an initial condition for constant pressure molecular dynamics (NpT MD).
(iv) NpT MD simulations (2−3 ns at 1 atm) were done at 100 K, then heated at 200 K, and so on up to the normal boiling point of each liquid to ensure proper melting (more simulation details given below), followed by sequential cooling to the normal freezing point of each liquid to yield equilibrated systems and mean lattice parameters for subsequent constant energy/volume (NVE) MD at several temperatures.
(v) NVE MD simulations (1 ns constant volume/temperature (NVT) equilibration, 5 ns NVE production) at various liquid temperatures to produce dynamical information such as orientational correlation functions (details given below) free from thermostats or barostats that may contaminate dynamics.

Table S1 in the Supporting Information contains useful information for building these liquid systems such as CSD name, numbers of molecules, and mean lattice parameters for selected temperatures.

We built three-dimensional initial conditions for pentamer-based materials by first placing pentamers in sheets of five pentamers with reasonable van der Waals distances between adjacent pentamers (see Figure 2 in ref 14 and then by stacking six sheets with about 10 Å between each sheet, yielding initially ordered structures, including 150 azole molecules. Each of these structures was subjected to a sequence of simulations similar to those described above for the neat liquid systems, beginning with energy minimization at constant volume in orthorhombic cells ($a \neq b \neq c$) to produce initial configurations for NpT MD simulations. We then performed a series of NpT MD simulations (2−3 ns) at 1 atm equilibrating at 200 K, then equilibrating to 300 K, and so on up to 900 K to produce an equilibrated melt for each of the five pentamer-based materials.

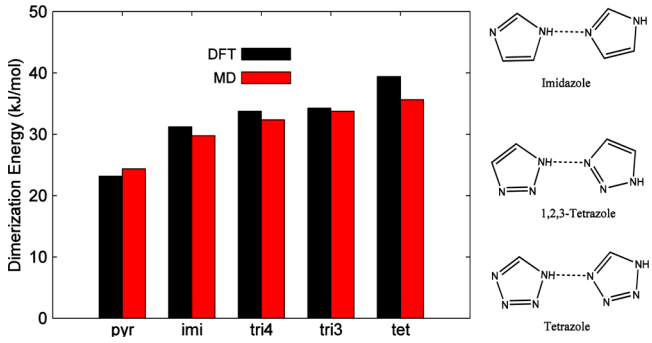

Figure 2. Dimerization energies calculated using MD (GAFF) (azoles: pyrazole, imidazole, 1,2,4-triazole, 1,2,3-triazole, and tetrazole) (red) and DFT (B3LYP/6-311G(d,p)-BSSE) (black). pyr = pyrazole; imi = imidazole; tri4 = 1,2,4-triazole; tri3 = 1,2,3-triazole; tet = tetrazole.

We then cooled it sequentially from 900 to 800 K, from 800 to 700 K, and so on back to 200 K to generate reasonable models of the likely disordered materials that synthetic chemists may fabricate from such oligomers. We expect these materials to cool to disordered, glassy states[47] because of the entangling hydrogen bond clusters that are found to grow with decreasing temperature. These equilibrated systems and mean lattice parameters were then used for subsequent NVE MD simulations (1 ns NVT equilibration, 5−30 ns NVE production), which we used to extract dynamical information for the pentamer-based materials for comparison with results from corresponding nonpentamer liquid systems. Table S2 contains mean lattice parameters for each pentamer-based material at 300 K.

Simulation Details. The general Amber force field (GAFF)[48,49] was initially chosen to describe intra- and intermolecular interactions for all systems studied. The intramolecular bonded interactions contain bond stretching, angular bending, and dihedral twisting. Nonbonded interactions include electrostatic and van der Waals (VDW) terms. The functions employed by GAFF can be written as follows:

$$V = \sum_{N_b} \frac{1}{2} k_b (r - r_o)^2 + \sum_{N_a} \frac{1}{2} k_a (\theta - \theta_o)^2 + \sum_{N_d} k_d [1 + \cos(m\phi - \phi_o)] + \sum_{N_{nb}} \left\{ \frac{q_i q_j}{r_{ij}} + 4\varepsilon_{ij} \left[\left(\frac{\sigma_{ij}}{r_{ij}} \right)^{12} - \left(\frac{\sigma_{ij}}{r_{ij}} \right)^{6} \right] \right\} \quad (1)$$

where r, θ, and φ are the intramolecular bond length, valence angle, and dihedral angle, respectively, and q is the atomic partial charge. ε_{ij} and σ_{ij} are the van der Waals parameters used for intermolecular interactions. The partial atomic charges of isolated azole molecules and azole monomers (repeat units) were determined by fitting point charges to the electrostatic potential[50,51] obtained using B3LYP/6-311G(d,p) in Gaussian09.[52] Atomic point charges on tethered systems and in tethered functional groups are reported in Table S3.

As a fundamental test of this force field, we calculated binding energies of gas-phase homodimers of functional group molecules (without linker or backbone) optimized using B3LYP/6-311G(d,p) in Gaussian09 with single-point corrections for basis set superposition error (BSSE) in dimerization energies using the counterpoise method.[53] These dimerization

DOI: 10.1021/acs.jpcb.6b07148
J. Phys. Chem. B 2016, 120, 10411−10419

energies ($\Delta E = |E_{dimer} - 2E_{monomer}|$) were taken as measures of hydrogen bonding strengths for direct comparison with optimized GAFF homodimerization energies computed with cell parameters large enough (15−20 Å) to minimize interactions among periodic images in DL_Poly_2. The resulting comparison of dimerization energies (Figure 2) shows that the collection of force fields used herein captures hydrogen bond strengths for all five systems. In addition, we produce liquid densities close to the experimental values (see Figure 3 for simulated liquid and pentamer densities versus

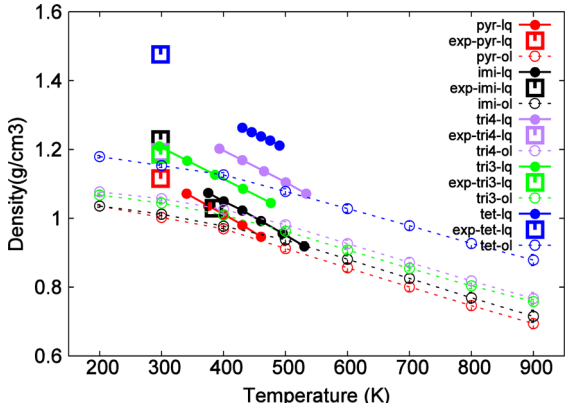

Figure 3. Densities of neat liquid azoles (solid circle) and pentamers (open circle) as a function of temperature. Experimental solid azole densities at 298 K (squares) are shown, giving plausible agreement with extrapolated equations of state for the simulated liquids.

temperature for various systems). The intermolecular hydrogen bond lengths (N−H) from B3LYP/6-311G(d,p) and DL_Poly_2 dimer optimizations are given in Table S4, also showing broad agreement. As such, the force fields used herein capture the essential characteristics of hydrogen bonding in the five systems studied below.

All MD simulations reported herein used the velocity-Verlet algorithm to integrate Newton's equations with a 1 fs time step. All simulations were performed using three-dimensional periodic boundary conditions. Long-range electrostatic interactions were calculated with Ewald lattice summation using a convergence parameter of 10^{-6}, while van der Waals interactions were shifted and cut off with a radius of 10 Å. MD simulations in the NpT ensemble were performed using the Nose-Hoover thermostat (1 ps relaxation time) and barostat (2 ps relaxation time)[54] in DL_Poly_2. Each NVE simulation was (i) initiated with an equilibrated configuration and mean lattice parameters from a corresponding NpT simulation, (ii) equilibrated in the NVT ensemble for 1 ns by scaling velocities every 50 steps, and (iii) run in the NVE ensemble for another 5−30 ns (depending on the dynamics of the system in question) without a thermostat or barostat. Production simulations were carried out on our Beowulf cluster using 24 2.53 GHz processors (8 processors/node) and also on the Massachusetts Green High Performance Computing Center (MGHPCC) cluster, both requiring roughly 45 CPU hours per temperature. In what follows, we describe the methods used to characterize hydrogen bond networks and reorientation dynamics in the neat liquids and pentamer-based materials studied below.

Cluster Statistics. In this work, as in our previous work,[14] the hydrogen bond is defined when the intermolecular distance between (N)H···N species is less than 2.5 Å. Other authors have considered multidimensional definitions of hydrogen bonds, including bond lengths, angles, and energies.[55] For example, when considering the O−H−O bond angle for hydrogen bonding in water, Matsumoto suggested angles greater than ∼90° as a defining characteristic of hydrogen bonding. Our simulations (Figure S2) show that, for the overwhelming majority of configurations with intermolecular H···N distance above 2.5 A, the NHN angle is already above 90°. As such, the simple distance criterion for hydrogen bonding used below was found to be sufficient. The number of hydrogen bonds per amphiprotic molecule/group was computed for liquid/pentamer systems (Figure S4) by investigating configurations every 50 fs. Hydrogen bond lifetimes were calculated by recording initial and final times for each hydrogen bond. All the mean hydrogen bond lifetimes simulated herein were found to exceed 200 fs (Figure 4),

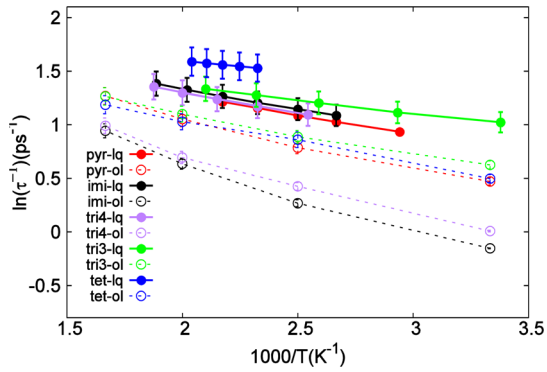

Figure 4. Arrhenius dependence of hydrogen bond lifetimes for neat liquid azoles (solid circles) and azole pentamers (open circles). Apparent activation energies are shown in Table S5.

indicating that examining trajectories every 50 fs is sufficient to capture most of the hydrogen bond dynamics. Hydrogen bond lifetime activation energies were extracted by fitting the Arrhenius equation to the temperature dependence of mean hydrogen bond lifetimes.

Collective hydrogen bond networks can be thought of as fluctuating clusters, whose sizes can be computed by analyzing the connectivity matrix C designed by Sevick.[56] If two molecules (i,j) are directly connected by a hydrogen bond, the $i-j$th matrix elements $C_{i,j} = C_{j,i} = 1$; otherwise, they take the value zero. When the jth molecule is also directly hydrogen bonded to another molecule, k, then the $i-k$ pair is indirectly connected, and the matrix elements take the value $C_{i,k} = C_{k,i} = 1$. From analysis of the connectivity matrix, we obtain hydrogen bond cluster sizes in neat liquids and pentamer systems.

Orientational Dynamics. The orientational dynamics of various molecular segments were investigated by the following orientational autocorrelation function:

$$C(t) = \langle N(0) \times N(t) \rangle - \langle N \rangle \times \langle N \rangle \quad (2)$$

where $N(t)$ is the unit vector normal to the ring of an amphiprotic molecule or a functional group at time t. The order parameter $|\langle N \rangle|$ provides information on the liquid-to-glass transition as temperature is decreased in pentamer-based materials. As in our previous work,[15] we found it more convenient to separately analyze order parameters and correlation functions. We also studied order parameters and correlation functions of backbone and linker groups using end-to-end unit vectors of carbon chains[15] to study the temperature

DOI: 10.1021/acs.jpcb.6b07148
J. Phys. Chem. B 2016, 120, 10411−10419

dependence and hierarchy of backbone, linker, and functional group motions. As such, we computed and fitted orientational correlation functions as shown in eq 3 below:

$$C(t) = \langle N(0)\cdot N(t)\rangle$$

$$C(t) = b + a\mathrm{e}^{-t/\tau_1} + (1-a)\mathrm{e}^{-t/\tau_2} \quad (3)$$

The first lifetime (τ_1) in eq 3 is related to relatively rapid librations (hindered rotor vibrations) of a given molecular segment, while the second lifetime (τ_2) is the time associated with complete orientational randomization.[5] Activation energies for orientational randomization were obtained by fitting the Arrhenius equation to the temperature dependence of reorientation times (τ_2) for liquid molecules, pentamer backbones, linkers, and functional groups.

3. RESULTS AND DISCUSSION

Here, we report a hierarchy of simulated properties, including the calculated thermodynamic densities of liquid and pentamer systems from NpT simulations, hydrogen bonding lifetimes, cluster sizes, orientational order parameters, orientational correlation functions, and reorientation rates of various molecular segments from NVE simulations of the neat liquids and pentamer-based materials.

Density Equation of State. To test the thermodynamic predictions of the force fields, we show in Figure 3 the densities of azole pentamer systems over the range of 200−900 K and neat liquids in each liquid temperature range. The experimental densities of liquid imidazole at 384 K (black square) and liquid 1,2,3-triazole at 298 K (green square) agree well with our simulated values. The experimental densities of solid azoles at 298 K (squares) are shown as reference values. The temperature dependencies of pentamer densities are weaker than those of the liquids, which may be due to the glassy state of pentamer materials at lower temperatures. The radial distribution function plots for intermolecular H···N atom pairs in neat liquids at 300 K are shown in Figure S3, and their peak distances are tabulated in Table S4, which agree well with available literature values.

Hydrogen Bond Numbers and Lifetimes. Figure S4 shows the numbers of hydrogen bonds as a function of temperature for neat liquids and pentamers relative to the total number of amphiprotic groups in each simulation. The pyrazole, 1,2,4-triazole, and tetrazole neat liquids in Figure S4 show similar (normalized) numbers of hydrogen bonds in corresponding tethered systems for which tethering has little effect on the number of hydrogen bonds. For imidazole, tethering appears to increase the number of hydrogen bonds, as found in our previous work, because connecting imidazole to alkane linkers increases the magnitudes of N and H partial charges in hydrogen bonded NH atoms.[14,15,33] However, for 1,2,3-triazole, tethering appears to decrease the number of hydrogen bonds, even though tethering also increases the magnitudes of N/H partial charges, and imidazole-like hydrogen bond networks are possible with 1,2,3-triazole.[36] The key difference for 1,2,3-triazole is its linker connection point (Figure 1), which impacts the nature of hydrogen bond network connectivities. The variation in numbers of hydrogen bonds with temperature is too weak to extract apparent activation energies for these systems, prompting us to turn to hydrogen bond lifetimes.

Figure 4 shows mean hydrogen lifetimes for liquids and pentamers versus temperature. Hydrogen bonds were found to exhibit lifetimes in pentamers longer than those in corresponding liquids, indicating that the topological constraints from tethering enhance hydrogen bond lifetimes. The apparent activation energies associated with these hydrogen bond lifetimes are slightly larger for pentamers than for neat liquids. Both liquid and pentamer lifetime activation energies are much less than typical apparent activation energies extracted from reorientation rates of functional groups,[29,30] indicating that the simple act of breaking individual hydrogen bonds does not account for the energetics of functional group reorientation.

Hydrogen Bond Cluster Sizes. We now turn to more collective properties of hydrogen bonding in these systems, focusing first on hydrogen bond cluster sizes. Figure 5 shows

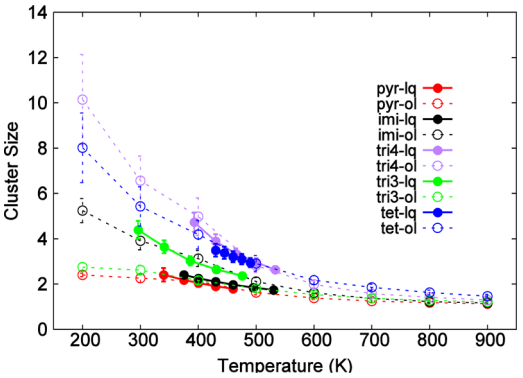

Figure 5. Mean hydrogen bond cluster sizes versus temperature for neat azole liquids (solid circles) and azole pentamers (open circles).

mean hydrogen bond cluster sizes as a function of temperature for the neat liquids and pentamers. The triazole and tetrazole systems show clusters larger than those in imidazole and pyrazole neat liquids, likely due to their multiple proton acceptors. As with the number of hydrogen bonds, there is no single effect from tethering on cluster sizes. Indeed, for imidazole, tethering extends clusters, while for 1,2,3-triazole, tethering reduces cluster sizes down to the values seen for pyrazole. These trends in cluster sizes mirror those found above in the numbers of hydrogen bonds.

Functional Group, Linker, and Backbone Orientational Order Parameters. Figure 6 shows the functional group orientational order parameter in pentamer materials as a function of temperature over the range of 200−900 K. Figures S5 and S6 show the same for linker and backbone segments. Order parameters computed for liquid systems (data not

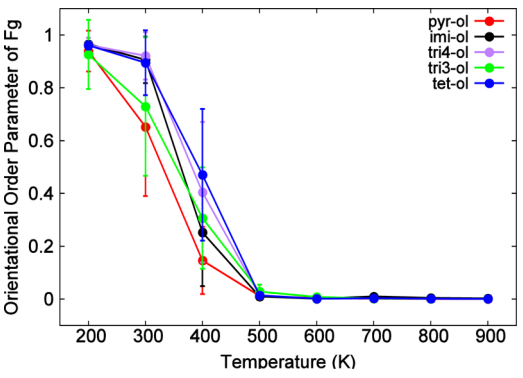

Figure 6. Orientational order parameter versus temperature for functional groups in pentamer materials.

DOI: 10.1021/acs.jpcb.6b07148
J. Phys. Chem. B 2016, 120, 10411−10419

shown) were found to vanish within statistical error of a few percent. If we define liquid-like motion by an order parameter less than 0.1, we see in Figure 6 that the azole functional groups achieve liquid-like motion at 500 K. Similar trends are seen in Figures S5 and S6 for linker and backbone segments; all of the azole-based materials achieve linker/backbone orientational randomization at 600 K. The vanishing of these order parameters shows that the initial order assumed in our construction of these tethered systems has been destroyed by sufficient heating.

Figures 6, S5, and S6 show that trends in backbone orientational order parameters related to the glass transition temperature (T_g) of polymers[57] also track with trends in linkers and functional groups. This finding may explain why proton conductivities often anticorrelate with polymer T_g values,[22] as lower T_g values correspond to higher backbone flexibilities, which our present findings suggest may also correlate with enhanced functional group and linker motion.

Orientational Correlation Functions (OCFs). OCFs for liquid molecules, pentamer functional groups, linkers, and backbone segments were calculated for all five functionalities and for a variety of temperatures over relevant ranges. Here, we report on selected OCFs. Figure 7 shows OCFs for tetrazole

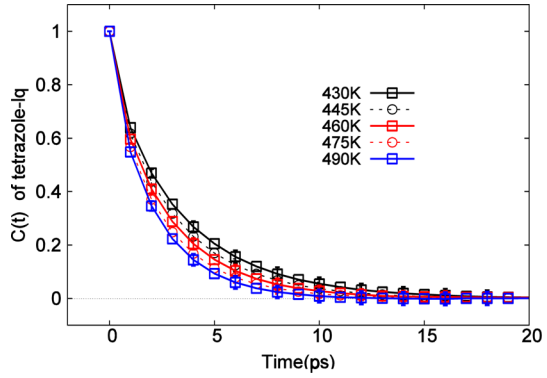

Figure 7. Orientational correlation functions of liquid tetrazole at various temperatures.

liquids at various temperatures. All OCFs for liquid molecules were found to exhibit complete decay, consistent with vanishing order parameters. Figure 8 shows OCFs for tethered tetrazole functional groups over the range of 200–900 K, revealing distinct liquid-like regimes at high temperatures and glassy

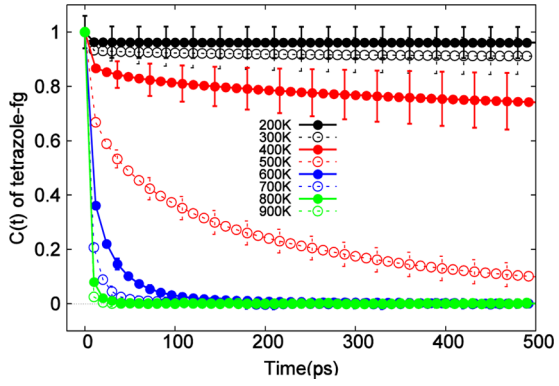

Figure 8. Orientational correlation functions of tetrazole functional groups in pentamers at various temperatures.

regimes at low temperatures. Figures S7 and S8 show OCFs for backbone and linker segments, respectively, in tetrazole-based pentamers over a range of temperatures, indicating the same liquid-like and glassy regimes. All OCFs for liquids and pentamers (above 500 K) were fitted to biexponential functions; reorientation times (τ_2) were extracted at various temperatures, and apparent activation energies were computed (Table S6) by Arrhenius analysis (Figures S9–S11). The pentamer motions below 500 K were too sluggish to be captured by our present computational resources.

An analysis of the distribution of time scales in the glassy systems may shed light on the experimental observation by Spiess and co-workers on the presence of both static and dynamic hydrogen bonding for tethered imidazole systems on NMR time scales.[29] From our simulations of tethered imidazole at 400 K, we find a wide distribution of rotational time scales, ranging from 50 ps to 26 ns and exhibiting a distribution similar to log-normal in shape (see Figure S12 for raw data).[15] In an effort to understand the origin of this distribution of time scales, we first pursued a correlation with a measure of local density around each functional group based on the hypothesis that local density fluctuations may hamper or facilitate functional group rotation. We computed the number of atoms in a sphere of given radius (considering radii from 4–13 Å) centered on each functional group and compared the resulting densities to the rotational time scales in Figure S12. No clear correlation emerged from this analysis (density data not shown), which revealed a surprisingly narrow distribution in local densities. We then pursued a correlation between rotational time scales of selected functional groups and their mean hydrogen bond lifetimes (Figure S13), which showed a good correlation. Despite this progress, the question of what local environmental and structural characteristics cause the wide distribution of rotational time scales and hydrogen bond lifetimes remains to be determined.

Here, we compare activation energies extracted from Arrhenius analyses of our simulated functional group reorientation rates (Figure 9) with activation energies measured

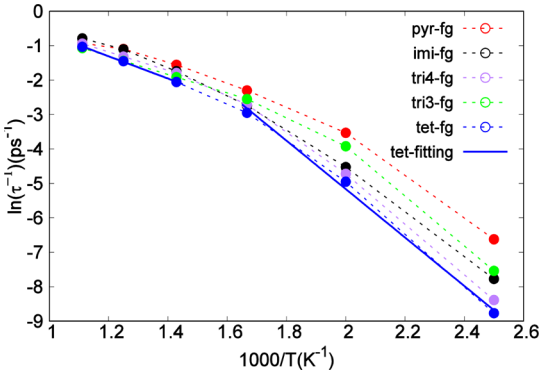

Figure 9. Arrhenius plot of reorientation times for amphiprotic groups in pentamers. The dashed lines are data, and the blue solid line is the linear fitting of tetrazole data.

via MAS NMR experiments. Akbey et al.[30] applied variable-temperature NMR to study solids composed of triazole groups tethered to a polysiloxane backbone via flexible linkers. They measured relaxation times associated with the orientational randomization of the triazole groups. The activation energies of these molecular reorientations at high temperatures ($T > 310$ K) and low temperatures ($260 < T < 300$ K) are shown in

DOI: 10.1021/acs.jpcb.6b07148
J. Phys. Chem. B 2016, 120, 10411–10419

Table 1, revealing very good agreement with our simulation results. We note that the MD simulations considered much broader temperature ranges because of the well-known time scale limitations of MD.

Table 1. Apparent Activation Energies (kJ/mol) of Triazole Reorientation Times from NMR (Ref 30) and Our Simulations for Tethered Triazole Oligomers at High (HT) and Low Temperature Ranges (LT)

name	E_a (HT)	E_a (LT)
Tri124	22.2 ± 0.1	59.7 ± 3.2
Tri123	22.1 ± 0.1	57.9 ± 4.3
Tri123[30]	30.7	58.3

Goward et al.[29] studied ethylene-oxide-tethered imidazole pairs (Imi-*n*EO) with high-resolution solid-state ^{1}H NMR, where *n* reflects the length of the ethylene-oxide linker. They characterized the local mobility of the hydrogen bonded protons as a function of temperature by their spin−spin relaxation (T_2^*) behavior. Although the tethering architectures of our model systems and the species considered by Goward et al. differ in detail, we can compare them based on the numbers of backbone and/or linker heavy atoms (carbons and oxygens) per imidazole in each respective oligomer molecule. In the Imi-1EO and Imi-5EO molecules, this ratio takes the values 3 and 9, respectively, while in our model architecture, the ratio equals 7. As such, we might expect the Imi-1EO and Imi-5EO behaviors to bracket that of our model system. Activation energies for imidazole orientational randomization measured from Imi-1EO and Imi-5EO are shown in Table 2. These values do indeed bracket our computed value for tethered imidazole, as expected.

Table 2. Apparent Activation Energies (kJ/mol) of Imidazole Reorientation Times from NMR (Ref 29) and Our Simulations for Tethered Imidazole Oligomers in the Solid State

name	E_a	chain atom/number of imidazoles[a]
Imi	52.9 ± 2.9	7
Imi-1EO[29]	48	3
Imi-5EO[29]	60	9

[a]Ratio between the number of backbone and linker heavy atoms to the number of imidazoles.

Figure 10 pursues the possibility of a correlation between reorientation activation energies of functional groups in pentamer systems and hydrogen bond energies from DFT calculations on gas-phase dimers (Table S6). Such a correlation could simplify the process of obtaining design parameters for new PEMs. Figure 10 reveals that data from pyrazole, the two triazoles, and tetrazole lie close to a correlation line with slope 0.61 ± 0.11, while data from imidazole represent a statistically significant outlier from this correlation. Indeed, the apparent activation energy for imidazole functional group orientational randomization in the pentamer system, 27.7 kJ/mol, is 6.3 kJ/mol higher than that expected from this line (21.4 kJ/mol). Our results above suggest that two factors may conspire to explain this behavior of imidazole: (i) key charges on hydrogen bonding atoms N and H intensify upon tethering, and (ii) the structure of imidazole allows for "linear" and not "zig-zag" hydrogen bonding clusters. Linear hydrogen bond clusters are postulated to pack more effectively and thus be more stable.[36]

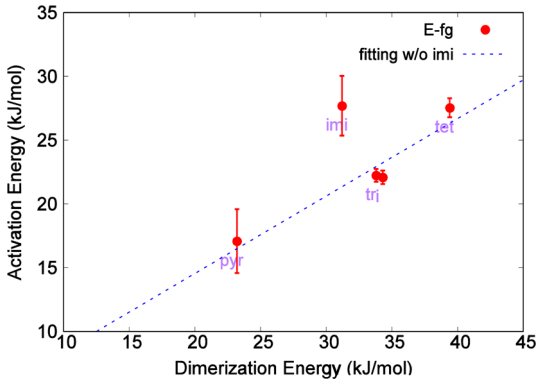

Figure 10. Graph of reorientation (solid line) activation energies from functional groups in pentamers (red points) versus DFT-computed hydrogen bond energies on the *x*-axis (B3LYP/6-311G(d,p)-BSSE, normalized by number of bonds) showing that a linear correlation (R^2 = 0.94) exists between the gas-phase dimer energy and bulk rotation barrier in pyrazole, triazoles, and tetrazole.

Imidazole is the only azole considered herein with both of these properties. Despite this exception, the correlation in Figure 10 provides a potentially useful design parameter for next-generation PEMs.

4. SUMMARY AND CONCLUSION

We simulated structures and dynamics of hydrogen bonding in amphiprotic groups, including azole bases (pyrazole, imidazole, 1,2,4-triazole, 1,2,3-triazole, and tetrazole), as neat molecular liquids and also tethered in pentamer brush-like structures. Each monomer of the pentamer brush includes one amphiprotic functional group connected to a butyl backbone via a propyl linker. We investigated how tethering and varying functional groups influence sizes of hydrogen bond networks and rates of reorientation dynamics, both factors thought to affect proton conduction.

We employed the DL_Poly_2 molecular dynamics suite with the GAFF force field for azoles to simulate pentamer systems for temperatures in the range of 200−900 K and neat liquids under liquid temperatures at a pressure of 1 atm. Accuracy tests of the force fields used herein showed good agreement on hydrogen bond strengths and bond lengths when compared to density functional theory calculations on gas-phase dimers. NpT MD simulations were used to compute thermodynamic equations of state for the five liquids and five pentamer materials, giving good agreement for systems where experiment density data are available. NVE MD simulations were launched from equilibrated NpT configurations to compute properties such as sizes of hydrogen bond clusters; orientational order parameters and orientational correlation functions (OCFs) characterizing liquids, tethered functional groups, linkers, and backbones; and reorientation times and associated activation energies.

In general, the tethered systems retain roughly the same size of hydrogen bond cluster as do liquids at the same temperature but with longer hydrogen lifetimes. All the pentamer-based materials studied above exhibit a liquid to glassy-solid transition upon cooling, with glassy solids forming around 500 K. Functional-group reorientation rates were found to decrease dramatically upon tethering, and reorientation barriers increased upon tethering. The activation energies associated with orientational randomization of functional groups agree well with NMR data for imidazole oligomers tethered with

DOI: 10.1021/acs.jpcb.6b07148
J. Phys. Chem. B 2016, 120, 10411−10419

ethylene oxide linkers. We also found good agreement with NMR data for low- and high-temperature activation energies associated with orientational randomization of tethered 1,2,3-triazole systems. Finally, we found a linear correlation between gas-phase hydrogen bond energies and tethered-functional group reorientation barriers for all azoles except for imidazole, which exhibits a rotational barrier ∼6 kJ/mol above the correlation-line value because of both charges and molecular structure allowing more stable packing of hydrogen bonded clusters.

Future simulations of proton diffusion in untethered and tethered amphiprotic groups in liquid and glassy systems are necessary to understand more fully the competition between hydrogen bond cluster size and functional group reorientation rate in controlling proton conduction.

■ ASSOCIATED CONTENT

Supporting Information

The Supporting Information is available free of charge on the ACS Publications website at DOI: 10.1021/acs.jpcb.6b07148.

Additional simulation data (PDF)

■ AUTHOR INFORMATION

Corresponding Author

*E-mail: auerbach@umass.edu; Phone: 413-545-1240.

Notes

The authors declare no competing financial interest.

■ ACKNOWLEDGMENTS

The authors thank Brett Clinton for initial simulations on these many functional groups. We also thank the Massachusetts Green High Performance Computing Center (MGHPCC) for generous access to computational resources.

■ REFERENCES

(1) Kreuer, K.-D. D.; Paddison, S. J.; Spohr, E.; Schuster, M. Transport in Proton Conductors for Fuel-Cell Applications: Simulations, Elementary Reactions, and Phenomenology. *Chem. Rev.* **2004**, *104*, 4637−4678.

(2) Scharfenberger, G.; Meyer, W. H.; Wegner, G.; Schuster, M.; Kreuer, K.-D.; Maier, J. Anhydrous Polymeric Proton Conductors Based on Imidazole Functionalized Polysiloxane. *Fuel Cells* **2006**, *6*, 237−250.

(3) Herz, H. G.; Kreuer, K. D.; Maier, J.; Scharfenberger, G.; Schuster, M. F. H.; Meyer, W. H. New Fully Polymeric Proton Solvents With High Proton Mobility. *Electrochim. Acta* **2003**, *48*, 2165−2171.

(4) Granados-Focil, S.; Woudenberg, R. C.; Yavuzcetin, O.; Tuominen, M. T.; Coughlin, E. B. Water-Free Proton-Conducting Polysiloxanes: A Study on the Effect of Heterocycle Structure. *Macromolecules* **2007**, *40*, 8708−8713.

(5) Spohr, E.; Commer, P.; Kornyshev, A. A. Enhancing Proton Mobility in Polymer Electrolyte Membranes: Lessons from Molecular Dynamics Simulations. *J. Phys. Chem. B* **2002**, *106*, 10560−10569.

(6) López, G. E.; Colón-Díaz, I.; Cruz, A.; Ghosh, S.; Nicholls, S. B.; Viswanathan, U.; Hardy, J. A.; Auerbach, S. M. Modeling Nonaqueous Proton Wires Built from Helical Peptides: Biased Proton Transfer Driven by Helical Dipoles. *J. Phys. Chem. A* **2012**, *116*, 1283−1288.

(7) Heberle, J. Proton Transfer Reactions Across Bacteriorhodopsin And Along The Membrane. *Biochim. Biophys. Acta, Bioenerg.* **2000**, *1458*, 135−147.

(8) Peng, Y.; Voth, G. A. Expanding The View Of Proton Pumping In Cytochrome C Oxidase Through Computer Simulation. *Biochim. Biophys. Acta, Bioenerg.* **2012**, *1817*, 518−525.

(9) Agarwal, V.; Huber, G. W.; Conner, W. C.; Auerbach, S. M. Simulating Infrared Spectra And Hydrogen Bonding In Cellulose Ibeta At Elevated Temperatures. *J. Chem. Phys.* **2011**, *135*, 134506−134513.

(10) Agarwal, V.; Dauenhauer, P. J.; Huber, G. W.; Auerbach, S. M.; Scott, M.; Cell, S. S. Ab Initio Dynamics of Cellulose Pyrolysis: Nascent Decomposition Pathways at 327 and 600 °C. *J. Am. Chem. Soc.* **2012**, *134*, 14958−14972.

(11) Shih, R.-S.; Lu, C.-H.; Kuo, S.-W.; Chang, F.-C. Hydrogen Bond-Mediated Self-Assembly of Polyhedral Oligomeric Silsesquioxane-Based Supramolecules. *J. Phys. Chem. C* **2010**, *114*, 12855−12862.

(12) Zhao, Y.; Stejskal, J.; Wang, J. Towards Directional Assembly Of Hierarchical Structures: Aniline Oligomers As The Model Precursors. *Nanoscale* **2013**, *5*, 2620−2626.

(13) de Grotthuss, C. Theory Of Decomposition Of Liquids By Electrical Currents. *Ann. Chim.(Paris)* **1806**, *58*, 54−74.

(14) Harvey, J. A.; Basak, D.; Venkataraman, D.; Auerbach, S. M. Simulating Hydrogen-Bond Clustering And Phase Behaviour Of Imidazole Oligomers. *Mol. Phys.* **2012**, *110*, 37−41.

(15) Harvey, J. A.; Auerbach, S. M. Simulating Hydrogen-Bond Structure and Dynamics in Glassy Solids Composed of Imidazole Oligomers. *J. Phys. Chem. B* **2014**, *118*, 7609−7617.

(16) Li, S.; Fried, J. R.; Colebrook, J.; Burkhardt, J. Molecular simulations of neat, hydrated, and phosphoric acid-doped polybenzimidazoles. Part 1: Poly(2,2-M-Phenylene-5,5′-Bibenzimidazole) (PBI), Poly(2,5-Benzimidazole) (ABPBI), And Poly(P-Phenylene Benzobisimidazole) (PBDI). *Polymer* **2010**, *51*, 5640−5648.

(17) Kwiendacz, J.; Boczar, M.; Wójcik, M. J. Car−Parrinello Molecular Dynamics Simulations Of Infrared Spectra Of Crystalline Imidazole. *Chem. Phys. Lett.* **2011**, *501*, 623−627.

(18) Jiménez-García, L.; Kaltbeitzel, A.; Pisula, W.; Gutmann, J. S.; Klapper, M.; Müllen, K. Phosphonated Hexaphenylbenzene: A Crystalline Proton Conductor. *Angew. Chem., Int. Ed.* **2009**, *48*, 9951−9953.

(19) Iannuzzi, M. Proton Transfer In Imidazole-Based Molecular Crystals. *J. Chem. Phys.* **2006**, *124*, 204710.

(20) Zhou, Z.; Li, S.; Zhang, Y.; Liu, M.; Li, W. Promotion Of Proton Conduction In Polymer Electrolyte Membranes By 1H-1,2,3-Triazole. *J. Am. Chem. Soc.* **2005**, *127*, 10824−10825.

(21) Narayanan, S. R.; Yen, S.-P.; Liu, L.; Greenbaum, S. G. Anhydrous Proton-Conducting Polymeric Electrolytes For Fuel Cells. *J. Phys. Chem. B* **2006**, *110*, 3942−3948.

(22) Yamada, M.; Honma, I. Anhydrous Proton Conducting Polymer Electrolytes Based On Poly (Vinylphosphonic Acid)-Heterocycle Composite Material. *Polymer* **2005**, *46*, 2986−2992.

(23) Chen, H.; Yan, T.; Voth, G. A. A Computer Simulation Model For Proton Transport In Liquid Imidazole. *J. Phys. Chem. A* **2009**, *113*, 4507−4517.

(24) Chelli, R.; Righini, R.; Califano, S.; Chimica, D.; Uni, V.; Lastruccia, V.; Fiorentino, S. Structure of Liquid Formic Acid Investigated by First Principle and Classical Molecular Dynamics Simulations. *J. Phys. Chem. B* **2005**, *109*, 17006−17013.

(25) Kreuer, K. D.; Fuchs, A.; Ise, M.; Spaeth, M.; Maier, J. Imidazole And Pyrazole-Based Proton Conducting Polymers And Liquids. *Electrochim. Acta* **1998**, *43*, 1281−1288.

(26) Petersen, M. K.; Voth, G. A. Characterization Of The Solvation And Transport Of The Hydrated Proton In The Perfluorosulfonic Acid Membrane Nafion. *J. Phys. Chem. B* **2006**, *110*, 18594−18600.

(27) Munch, W.; Kreuer, K.-D.; Silvestri, W.; Maier, J.; Seifert, G.; Münch, W.; Kreuer, K.-D.; Silvestri, W.; Maier, J.; Seifert, G. The Diffusion Mechanism Of An Excess Proton In Imidazole Molecule Chains: First Results Of An Ab Initio Molecular Dynamics Study. *Solid State Ionics* **2001**, *145*, 437−443.

(28) Gaigeot, M.-P.; Jarland, R. P. A.; Sprik, M. Ab Initio Molecular Dynamics Study of Uracil in Aqueous Solution. *J. Phys. Chem. B* **2004**, *108*, 7458−7467.

(29) Goward, G. R.; Schuster, M. F. H.; Sebastiani, D.; Schnell, I.; Spiess, H. W. High-Resolution Solid-State NMR Studies of Imidazole-Based Proton Conductors: Structure Motifs and Chemical Exchange from 1H NMR. *J. Phys. Chem. B* **2002**, *106*, 9322−9334.

(30) Akbey, Ü.; Granados-Focil, S.; Coughlin, E. B.; Graf, R.; Spiess, H. W. 1H Solid-State NMR Investigation of Structure and Dynamics of Anhydrous Proton Conducting Triazole-Functionalized Siloxane Polymers. *J. Phys. Chem. B* **2009**, *113*, 9151−9160.
(31) Steininger, H.; Schuster, M.; Kreuer, K. D.; Kaltbeitzel, A.; Bingöl, B.; Meyer, W. H.; Schauff, S.; Brunklaus, G.; Maier, J.; Spiess, H. W.; Bing, B.; Meyer, W. H.; Schauff, S.; Brunklaus, G.; Maier, J.; Spiess, H. W. Intermediate Temperature Proton Conductors For PEM Fuel Cells Based On Phosphonic Acid As Protogenic Group: A Progress Report. *Phys. Chem. Chem. Phys.* **2007**, *9*, 1764−1773.
(32) Lee, Y. J.; Bingol, B.; Murakhtina, T.; Sebastiani, D.; Meyer, W. H.; Wegner, G.; Spiess, H. W. High-Resolution Solid-State NMR Studies Of Poly(Vinyl Phosphonic Acid) Proton-Conducting Polymer: Molecular Structure And Proton Dynamics. *J. Phys. Chem. B* **2007**, *111*, 9711−9721.
(33) Viswanathan, U.; Basak, D.; Venkataraman, D.; Fermann, J. T.; Auerbach, S. M. Modeling Energy Landscapes Of Proton Motion In Nonaqueous, Tethered Proton Wires. *J. Phys. Chem. A* **2011**, *115*, 5423−5434.
(34) Milner, S. Polymer Brushes. *Science* **1991**, *251*, 905−914.
(35) Maupin, C. M.; Voth, G. A. Proton Transport In Carbonic Anhydrase: Insights From Molecular Simulation. *Biochim. Biophys. Acta, Proteins Proteomics* **2010**, *1804*, 332−341.
(36) Nagamani, C.; Versek, C.; Thorn, M.; Tuominen, M. T.; Thayumanavan, S. Proton Conduction In 1 H −1,2,3-Triazole Polymers: Imidazole-Like Or Pyrazole-Like? *J. Polym. Sci., Part A: Polym. Chem.* **2010**, *48*, 1851−1858.
(37) Martwiset, S.; Woudenberg, R.; Granadosfocil, S.; Yavuzcetin, O.; Tuominen, M.; Coughlin, E. Intrinsically Conducting Polymers And Copolymers Containing Triazole Moieties. *Solid State Ionics* **2007**, *178*, 1398−1403.
(38) Subbaraman, R.; Ghassemi, H.; Zawodzinski, T. A. 4, 5-dicyano-1 H-[1, 2, 3]-Triazole As A Proton Transport Facilitator For Polymer Electrolyte Membrane Fuel Cells. *J. Am. Chem. Soc.* **2007**, *129*, 2238−2239.
(39) Schuster, M.; Rager, T.; Noda, A.; Kreuer, K. D.; Maier, J. About the Choice of the Protogenic Group in PEM Separator Materials for Intermediate Temperature, Low Humidity Operation: A Critical Comparison of Sulfonic Acid, Phosphonic Acid and Imidazole Functionalized Model Compounds. *Fuel Cells* **2005**, *5*, 355−365.
(40) Paddison, S. J.; Kreuer, K.-D.; Maier, J. About The Choice Of The Protogenic Group In Polymer Electrolyte Membranes: Ab Initio Modelling Of Sulfonic Acid, Phosphonic Acid, And Imidazole Functionalized Alkanes. *Phys. Chem. Chem. Phys.* **2006**, *8*, 4530−4542.
(41) Pahari, S.; Roy, S. Proton Transport Mechanism Of Imidazole, Triazole And Phosphoric Acid Mixtures From Ab Initio Molecular Dynamics Simulations. *Phys. Chem. Chem. Phys.* **2015**, *17*, 30551−30559.
(42) Basak, D.; Versek, C.; Harvey, J. A.; Christensen, S.; Hillen, J.; Auerbach, S. M.; Tuominen, M. T.; Venkataraman, D. Enhanced Anhydrous Proton Conduction In Binary Mixtures Of 1H-Imidazole−1H-1,2,3-Triazole Based Compounds. *J. Mater. Chem.* **2012**, *22*, 20410−20417.
(43) Li, X.; Liao, S. Theoretical Study Of Proton Transfer In Triflic Acid/Water, Imidazole And Pyrazole Clusters. *J. Mol. Struct.: THEOCHEM* **2009**, *897*, 66−68.
(44) Schuster, M.; Meyer, W. H.; Wegner, G.; Herz, H. G.; Ise, M.; Kreuer, K. D.; Maier, J. Proton Mobility In Oligomer-Bound Proton Solvents: Imidazole Immobilization Via Flexible Spacers. *Solid State Ionics* **2001**, *145*, 85−92.
(45) Cavalcanti, W. L.; Portaluppi, D. F.; Joswig, J.-O. Preconditioning Immobilized Imidazole Arrays For Optimal Proton-Transfer Feasibility. *J. Chem. Phys.* **2010**, *133*, 104703.
(46) Allen, F. The Cambridge Structural Database: A Quarter Of A Million Crystal Structures And Rising. *Acta Crystallogr., Sect. B: Struct. Sci.* **2002**, *58*, 380−388.
(47) Baschnagel, J.; Binder, K.; Wittmann, H.-P. The Influence Of The Cooling Rate On The Glass Transition And The Glassy State In Three-Dimensional Dense Polymer Melts: A Monte Carlo Study. *J. Phys.: Condens. Matter* **1993**, *5*, 1597−1618.
(48) Wang, J. M.; Wolf, R. M.; Caldwell, J. W.; Kollman, P. A.; Case, D. A. Development And Testing Of A General Amber Force Field. *J. Comput. Chem.* **2004**, *25*, 1157−1174.
(49) Wang, J.; Wang, W.; Kollman, P. A.; Case, D. A. Automatic Atom Type And Bond Type Perception In Molecular Mechanical Calculations. *J. Mol. Graphics Modell.* **2006**, *25*, 247−260.
(50) Besler, B. H.; Merz, K. M.; Kollman, P. A. Atomic Charges Derived From Semiempirical Methods. *J. Comput. Chem.* **1990**, *11*, 431−439.
(51) Singh, U. C.; Kollman, P. A. An Approach To Computing Electrostatic Charges For Molecules. *J. Comput. Chem.* **1984**, *5*, 129−145.
(52) Frisch, M. J.; Trucks, G. W.; Schlegel, H. B.; Scuseria, G. E.; Robb, M. A.; Cheeseman, J. R.; Scalmani, G.; Barone, V.; Mennucci, B.; Petersson, G. A.; et al. *Gaussian 09*; Gaussian, Inc.: Wallingford, CT, 2009.
(53) Boys, S. F.; Bernardi, F. The Calculation Of Small Molecular Interactions By The Differences Of Separate Total Energies. Some Procedures With Reduced Errors. *Mol. Phys.* **1970**, *19*, 553−566.
(54) Melchionna, S.; Ciccotti, G.; Lee Holian, B.; Hoover, N. P. T. Dynamics For Systems Varying In Shape And Size. *Mol. Phys.* **1993**, *78*, 533−544.
(55) Matsumoto, M. Relevance Of Hydrogen Bond Definitions In Liquid Water. *J. Chem. Phys.* **2007**, *126*, 054503.
(56) Sevick, E. M.; Monson, P. A.; Ottino, J. M. Monte Carlo Calculations Of Cluster Statistics In Continuum Models Of Composite Morphology. *J. Chem. Phys.* **1988**, *88*, 1198−1206.
(57) Cowie, J. A. V. *Polymers: Chemistry and Physics of Modern Materials*; CRC Press: Boca Raton, FL, 2008.

DOI: 10.1021/acs.jpcb.6b07148
J. Phys. Chem. B 2016, 120, 10411−10419